

http://pubs.acs.org/journal/aesccq

# Comparison of the Yield and Chemical Composition of Secondary Organic Aerosol Generated from the OH and Cl Oxidation of Decamethylcyclopentasiloxane

Anita M. Avery,\* Mitchell W. Alton, Manjula R. Canagaratna, Jordan E. Krechmer, Donna T. Sueper, Nirvan Bhattacharyya, Lea Hildebrandt Ruiz, William H. Brune, and Andrew T. Lambe\*



Cite This: https://doi.org/10.1021/acsearthspacechem.2c00304



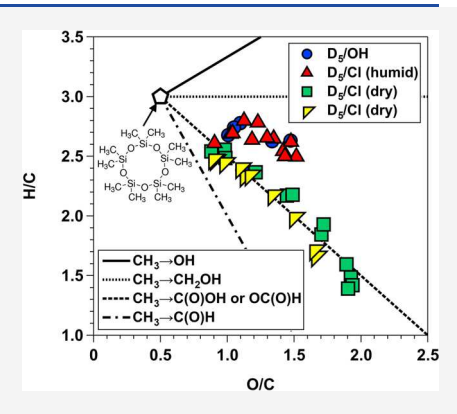
**ACCESS** I

III Metrics & More

Article Recommendations

Supporting Information

ABSTRACT: Cyclic volatile methyl siloxanes (cVMS) that are emitted from industrial processes and consumer products often dominate the burden of volatile organic compounds (VOCs) in occupied spaces. cVMS may contribute to oxygenated VOC and secondary organic aerosol (SOA) formation following oxidation by gas-phase radicals in both indoor and outdoor source regions. Several recent studies examined the SOA formation potential of decamethylcyclopentasiloxane (D<sub>5</sub>) following exposure to hydroxyl radicals (OH) and found that this reaction generates SOA in high yield following multiple days of oxidative aging. Chlorine atoms (Cl) may compete with OH for the oxidative loss of D<sub>5</sub> in indoor and outdoor source regions with active chlorine chemistry, but the SOA formation potential of D<sub>5</sub> + Cl reactions has not been studied. Here, we characterized the yield and chemical composition of SOA generated from Cl oxidation of D<sub>5</sub> in an oxidation flow reactor (OFR) under dry [relative humidity (RH) < 5%] and humid (RH = 40%) conditions and compared results to the yield and composition of SOA generated from OH oxidation of D<sub>5</sub>. D<sub>5</sub> was oxidized using



integrated OH and Cl exposures (OH<sub>exp</sub> and Cl<sub>exp</sub>) ranging from  $1.1 \times 10^{12}$  to  $8.2 \times 10^{12}$  cm<sup>-3</sup> s and from  $1.6 \times 10^{10}$  to  $1.6 \times 10^{12}$  cm<sup>-3</sup> s, respectively. Like OH, Cl facilitated multistep SOA oxidative aging over the range of OFR conditions that were studied, with maximum SOA mass yields of 1.5 and 1.3 obtained following OH and Cl oxidation of D<sub>5</sub> under humid conditions. These results suggest that indoor and outdoor source regions that are significantly influenced by chlorine chemistry may enhance the atmospheric SOA formation potential of D<sub>5</sub>.

KEYWORDS: volatile methyl siloxanes, secondary organic aerosol, hydroxyl radicals, chlorine atoms, oxidation flow reactor, aerosol mass spectrometry, proton transfer reaction mass spectrometry

## 1. INTRODUCTION

Cyclic volatile methyl siloxanes (cVMS), such as hexamethylcyclotrisiloxane (C<sub>6</sub>H<sub>18</sub>Si<sub>3</sub>O<sub>3</sub>, D<sub>3</sub>), octamethylcyclotetrasiloxane (C<sub>8</sub>H<sub>24</sub>Si<sub>4</sub>O<sub>4</sub>, D<sub>4</sub>), and decamethylcyclopentasiloxane  $(C_{10}H_{30}Si_5O_5, D_5)$ , are anthropogenic organosilicon compounds with Si-O-Si backbones that exist in the gas phase under typical atmospheric conditions. cVMS are emitted in large quantities from numerous industrial processes and consumer products and are often the most abundant class of volatile organic compounds (VOCs) in indoor densely occupied spaces. Additionally, cVMS, along with other chemical products, were only recently identified as important precursors to ozone and secondary organic aerosol (SOA) formation in polluted urban areas.<sup>2</sup> As such, recent studies have focused on the atmospheric chemistry of cVMS. D<sub>5</sub> is usually emitted in higher concentrations than other cVMS, with typical indoor and outdoor D<sub>5</sub> mixing ratios ranging from approximately 4 to 20 ppbv and from 0.4 to 20 pptv, respectively. 1,3-5

The atmospheric lifetime of  $D_5$  as a result of the reaction with the hydroxyl (OH) radical is approximately 3-5 days  $^{6,7}$  at a typical average ambient OH concentration of  $1.5 \times 10^6$  cm $^{-3.8}$  Important early-generation gas-phase  $D_5 + \text{OH}$  oxidation products include siloxanol/silanol compounds. Compounds with similar functional groups have been detected in laboratory  $D_5$  SOA particles. Given the lower volatility and higher emission factors of  $D_5$  relative to other VMS,  $D_5$  is a presumptive precursor to particulate Si in ambient aerosols.  $^{11-13}$  Recent studies investigating the OH oxidation of  $D_5$  and its early-generation oxidation products have shown that the yield of SOA increases significantly beyond  $\approx 10$  days of

Received: October 4, 2022 Revised: December 7, 2022 Accepted: December 14, 2022



atmospheric OH exposure.  $^{14-16}$  In addition to OH, chlorine atoms (Cl) may influence the atmospheric lifetime of  $D_5$  in certain source regions, including the marine boundary layer,  $^{17}$  polluted coastal cities,  $^{18}$  and indoors following bleach washing.  $^{19-21}$   $D_5$  reacts almost 2 orders of magnitude faster with Cl than with OH and generates similar early-generation gas-phase oxidation products.  $^7$  However, SOA generation following Cl oxidation of  $D_5$  has not been studied.

To investigate these knowledge gaps, we characterized the yield and chemical composition of laboratory SOA generated in an oxidation flow reactor (OFR) from the Cl oxidation of D<sub>5</sub>. First, we characterized the yield and chemical composition of SOA obtained from OH oxidation of D<sub>5</sub> and compared our results to previous studies. 14,16,22 OFRs use residence times that are on the order of minutes and oxidant concentrations that are typically 100-1000 times higher than ambient levels. Their ability to access photochemical aging time scales of up to several days was critical in previous studies examining D<sub>5</sub> + OH SOA formation as a result of the relatively long OH lifetime of D<sub>5</sub>. While these factors may make the chemistry and microphysics in the OFR somewhat different from the chemistry and microphysics in the atmosphere, <sup>23,24</sup> here, investigating D<sub>5</sub> Cl-SOA formation in an OFR enables a more direct comparison of the relative SOA yields obtained via OH and Cl oxidation (hereafter referred to as "OH-SOA" and "Cl-SOA", respectively). To first order, the yield and composition of Cl-SOA generated from other precursors appears to be similar whether it is generated at lower oxidant concentrations over longer exposure times in environmental chambers or higher oxidant concentrations over shorter exposure times in OFRs.<sup>25</sup>

# 2. EXPERIMENTAL SECTION

Experiments were conducted inside a Potential Aerosol Mass (PAM) OFR (Aerodyne Research, Inc.), which is a horizontal 13 L aluminum cylindrical chamber (46 cm long × 22 cm inner diameter) operated in continuous flow mode, with 6 L min<sup>-1</sup> flow through the reactor.<sup>25,26</sup> The corresponding calculated mean residence time in the OFR,  $au_{
m OFR}$ , was approximately 130 s. An electroconductive Teflon coating was applied to the OFR to improve chemical compatibility with halogen precursors while maintaining high transmission of gases and particles. <sup>25,27</sup> Two low-pressure mercury (Hg) lamps that were isolated from the sample flow using type 214 quartz sleeves were used to photolyze oxidant precursors. A fluorescent dimming ballast (IZT-2S28-D, Advance Transformer Co.) was used to regulate the current applied to the lamps. The ultraviolet (UV) irradiance was measured using a photodetector (TOCON-GaP6, sglux GmbH) and was varied across different experiments by changing the control voltage applied to the ballast between 1.5 and 10 volts of direct current (VDC). The corresponding actinic flux ranged from approximately  $1 \times 10^{14}$  to  $3 \times 10^{15}$  photons cm<sup>-2</sup> s<sup>-1,26,2</sup>

**2.1. Oxidant Generation.** 2.1.1. OH Production and Quantification. OH was generated from the combined photolysis of  $O_2$  and  $H_2O$  at  $\lambda=185$  nm plus photolysis of  $O_3$  at  $\lambda=254$  nm using two low-pressure ozone-producing UVC germicidal Hg lamps (GPH436T5VH/4P, Light Sources, Inc.); this method is hereafter referred to as "OFR185". Across all experiments, a mean relative humidity (RH) of  $40\pm1\%$  was established using a Nafion membrane humidifier (Perma Pure). The mean OFR temperature was  $28\pm2$  °C. The integrated OH exposure (OH<sub>exp</sub>) in the OFR, defined as the

product of the mean OH concentration and  $au_{
m OFR}$ , was calculated using an estimation equation  $^{26}$ 

$$\begin{split} \log[\text{OH}_{\text{exp}}] &= (10.098 + (0.15062 - 0.44244 \text{ OHR}_{\text{ext}}^{0.18041} \\ &+ 0.031146 \log[\text{O}_3 \times \text{OHR}_{\text{ext}}^{0.1672}]) \log[\text{O}_3] \\ &+ \log[\text{H}_2\text{O}]) + \log\!\left(\frac{\tau_{\text{OFR}}}{124}\right) \end{split} \tag{1}$$

where  $OHR_{ext}$  (external OH reactivity,  $s^{-1}$ ) is the product of the SOA precursor mixing ratio and its bimolecular OH rate coefficient (cm³ molecules $^{-1}$  s $^{-1}$ , hereafter "cm³ s $^{-1}$ ") and [O<sub>3</sub>] is the ozone concentration (molecules cm $^{-3}$ , hereafter "cm $^{-3}$ ") measured at the exit of the OFR. Over the range of conditions that were used, calculated OH<sub>exp</sub> values ranged from  $1.1 \times 10^{12}$  to  $8.2 \times 10^{12}$  cm $^{-3}$  s or from approximately 8 to 63 days of atmospheric oxidation at [OH] =  $1.5 \times 10^6$  cm $^{-3}$ .8 The estimated uncertainty in calculated OH<sub>exp</sub> values was  $\pm 50\%$ .

2.1.2. Cl Generation and Quantification. Cl was generated via photolysis of chlorine (Cl<sub>2</sub>) at  $\lambda = 369$  nm (Cl<sub>2</sub> +  $h\nu \rightarrow$ 2Cl) using two low-pressure UVA Hg lamps (F436T5/BLC/ 4P-369, LCD Lighting, Inc.) or photolysis of oxalyl chloride  $(C_2Cl_2O_2)$  at  $\lambda = 254$  or 313 nm  $(C_2Cl_2O_2 + h\nu \rightarrow 2Cl + \mu)$ 2CO) using two low-pressure UVC or UVB Hg lamps (GPH436TL/4P, Light Sources, Inc.; F436T5/BLC/4P-313, LCD Lighting, Inc.). Here, C<sub>2</sub>Cl<sub>2</sub>O<sub>2</sub> usage enabled the investigation of Cl-SOA oxidative aging in the absence of potential heterogeneous Cl2 uptake to the particles that could initiate secondary radical chain chemistry.<sup>29</sup> Photolysis of Cl-SOA at  $\lambda = 254$  nm was expected to be minor under the conditions that were used here.<sup>25</sup> These methods are hereafter referred to as "OFR369-iCl<sub>2</sub>" and "OFR254/313-iC<sub>2</sub>Cl<sub>2</sub>O<sub>2</sub>" where applicable ("i" = inject; thus, "iCl<sub>2</sub>" means that Cl<sub>2</sub> was the radical precursor injected into the OFR). The mean relative humidity (RH) was 4.9  $\pm$  0.2% at T = 29  $\pm$  2 °C during "dry" and 41  $\pm$  1% at T = 27  $\pm$  2 °C during "humid" OFR369-iCl<sub>2</sub> experiments. Similarly, the mean RH was 1.0  $\pm$ 0.1% at  $T = 25 \pm 2$  °C during OFR254/313-iC<sub>2</sub>Cl<sub>2</sub>O<sub>2</sub> experiments.

A compressed gas cylinder containing 0.1%  $Cl_2$  in  $N_2$  (Praxair) was used to supply  $Cl_2$  to the OFR. The  $Cl_2$  mixing ratio entering the OFR (set to 1.9 or 24.4 ppmv) was calculated from the  $Cl_2$  mixing ratio in the compressed gas mixture and the dilution ratio of  $15-200~\rm cm^3~min^{-1}$  into  $8000~\rm cm^3~min^{-1}$  carrier gas.  $C_2Cl_2O_2$  vapor was supplied to the OFR using a sealed permeation tube (EMPTY-HE, VICI) filled with liquid  $C_2Cl_2O_2$  and placed in a permeation tube oven that was heated to  $80~\rm ^{\circ}C$ . A carrier gas flow of  $100~\rm cm^3~min^{-1}$  zero air was used to transfer  $C_2Cl_2O_2$  vapor from the oven into the OFR. The calculated  $C_2Cl_2O_2$  mixing ratio (C) was 4.2 ppmv.  $^{25}$ 

Integrated Cl exposures ( $\text{Cl}_{\text{exp}}$ ) were characterized in offline calibration experiments by measuring the decay of  $O_3$  injected into the OFR following the reaction  $\text{Cl} + O_3 \rightarrow \text{ClO} + O_2$  and measured using an  $O_3$  analyzer (2B Technologies) as a function of lamp voltage; we assumed  $\pm 70\%$  uncertainty in  $\text{Cl}_{\text{exp}}$  values. O<sub>3</sub> concentrations were allowed to stabilize before initiating  $\text{Cl}_{\text{exp}}$  measurements, during which steady-state levels of  $O_3$  were obtained with the lamps turned off  $(O_{3,i})$ . Then, the lamps were turned on, and  $O_3$  concentrations were allowed to stabilize before being measured at illuminated steady-state conditions  $(O_{3,f})$  following reaction with Cl.  $\text{Cl}_{\text{exp}}$  at each condition was calculated using eq 2

$$Cl_{exp} = \frac{1}{k_{O_3}^{Cl}} - ln \left( \frac{[O_{3,f}]}{[O_{3,i}]} \right)$$
 (2)

where  $k_{\mathrm{O_3}}^{\mathrm{Cl}} = 1.21 \times 10^{-11} \ \mathrm{cm^3 \ s^{-1}}$  is the bimolecular Cl + O<sub>3</sub> reaction rate coefficient. Calculated Cl<sub>exp</sub> values in SOA experiments ranged from  $1.6 \times 10^{10}$  to  $1.6 \times 10^{12} \ \mathrm{cm^{-3}}$  s or from approximately 3 days to 10 months of atmospheric oxidation at [Cl] =  $6 \times 10^4 \ \mathrm{cm^{-3}}$ . These simple calculations should be interpreted as a rough estimate of the photochemical age in a representative source region with active Cl photochemistry and may vary by orders of magnitude elsewhere.  $^{32}$ 

2.2. Oxygenated Volatile Organic Compound (OVOC)/SOA Generation and Measurement. SOA particles were generated via the reaction of OH or Cl with D5 in the OFR. Liquid solutions containing  $D_5$  diluted to 10% (v/v) in carbon tetrachloride (CCl<sub>4</sub>) were injected into the OFR carrier gas flow at a liquid flow rate of 0.94  $\mu$ L h<sup>-1</sup> using a syringe pump. The D<sub>5</sub> mixing ratio with the corresponding D<sub>5</sub> mass concentration entering the OFR that was calculated from the liquid D<sub>5</sub> injection and dilution ratio into the carrier gas flow was 12 ppbv (182  $\mu$ g m<sup>-3</sup>). This value agrees with a mean  $D_5$  mixing ratio of 14.1  $\pm$  4.4 ppbv that was measured in a subset of experiments with a Vocus proton transfer reaction time-of-flight mass spectrometer<sup>33</sup> (hereafter referred to as "Vocus PTR") at the exit of the OFR. Similarly, the calculated CCl<sub>4</sub> mixing ratio in the OFR was 440 ppbv. At these conditions, the corresponding OHR<sub>ext</sub> and external Cl reactivity (ClR<sub>ext</sub>) values contributed by CCl<sub>4</sub> were <1  $\times$  10<sup>-7</sup> and 5  $\times$  10<sup>-12</sup> s<sup>-1.34,35</sup> These OHR<sub>ext</sub> and ClR<sub>ext</sub> values were negligible compared to those contributed by D<sub>5</sub> (0.6 and  $55 \text{ s}^{-1}$ ).

The Vocus PTR was operated using proton transfer  $(H_3O^+)$  reagent ion chemistry, which is selective toward compounds with proton affinities greater than that of  $H_2O$ , and its response to  $D_5$  was quantified by comparing to known injected quantities from a prepared dilute calibration gas cylinder (Apel-Riemer Environmental). The Vocus PTR was operated with an E/N value of 127, corresponding to an axial gradient of 607 V, a focusing ion molecule reaction region (fIMR) pressure of 2.2 mbar, and a fIMR temperature of 60 °C. The nominal resolving power of the instrument was 9770 at m/z 500 amu

Particle number concentrations and mobility size distributions were measured with a TSI scanning mobility particle sizer (SMPS). Ensemble aerosol mass spectra were measured with an Aerodyne long high-resolution time-of-flight aerosol mass spectrometer (L-ToF-AMS). In one subset of experiments, gas-phase OVOCs generated from OH/Cl oxidation of D<sub>5</sub> were characterized with the Vocus PTR. In another subset of experiments, SOA chemical composition was characterized using a Vocus Inlet for Aersols (hereafter VIA).<sup>36</sup> The VIA operates by passing the sample air through a honeycomb activated carbon denuder to remove all gas-phase constituents. The surviving aerosol is then evaporated in a Sulfinert-coated stainless-steel thermal desorption oven that was heated to 220 °C at a flow of 1.5 standard liters per minute to vaporize the particles prior to ionization and detection in the Vocus 2R PTR. The Vocus PTR was operated using the same source, voltage, and pressure conditions when in the gas phase or VIA mode.

**2.3. Analysis.** 2.3.1. L-ToF-AMS and Vocus PTR/VIA. L-ToF-AMS spectra were analyzed using ToF-AMS analysis software,<sup>37</sup> which yielded non-refractory organic and inorganic aerosol mass concentrations, high-resolution mass spectra, and, for the organic aerosol, hydrogen-to-carbon (H/C) and oxygen-to-carbon (O/C) ratios and abundances of the default  $C_xH_y^+$ ,  $C_xH_yO^+$ ,  $C_xH_yO_{>1}^+$ ,  $C_xH_ySi_zO_n^+$ , and  $Cl^+ + HCl^+$  ion groups. Elemental analysis was performed using the methods of Canagaratna et al. The AMS analysis software was modified to additionally calculate the oxygen-to-silicon (O/Si) and carbon-to-silicon (C/Si) ratios of the organic aerosol (Squirrel version 1.65D and Pika version 1.25D). These O/Si and C/Si values implicitly assume equal AMS sensitivity to C and Si, which has not been evaluated. Similarly, Vocus PTR and VIA spectra were analyzed using Tofware analysis software, which yielded high-resolution mass spectra and formulas of ions that were detected following proton transfer reactions between H<sub>3</sub>O<sup>+</sup> and sample analytes. The number of double bond equivalents (DBEs) was calculated for certain VIA analytes using eq 3

$$DBE = C + Si + 1 - H/2$$
 (3)

where C, Si, and H were the numbers of carbon, silicon, and hydrogen atoms in the compound formula. Using this definition,  $D_5$  has DBE = 1.

2.3.2. SOA Yields. SOA mass yields were calculated from the ratio of SOA mass formed to precursor gas reacted. The SOA mass was calculated from the integrated SMPS particle volume and the material density, which was calculated from H/C and O/C values extracted from the AMS spectra.<sup>39</sup> Because this calculation implicitly assumes that the particles were spherical, which was not independently verified, calculated SOA yield values reported in this paper represent upper limits. We estimated the fraction of precursor gas reacted from the product of  $OH_{exp}$  or  $Cl_{exp}$  and the bimolecular rate coefficients of D<sub>5</sub> + OH/Cl.<sup>7</sup> Our calculations suggested that >90% of D<sub>5</sub> reacted across the OFR conditions summarized in section 2.1. SOA yields were corrected for size-dependent particle wall losses in the OFR.40 Here, the particle wall loss correction factors ranged from 1.10 to 1.29 for mean volume-weighted particle mobility diameters ranging from approximately 125 to 45 nm. We assumed that low-volatility organic compound (LVOC) vapor wall losses were negligible compared to gasphase oxidative loss and condensation onto aerosols<sup>25,41,42</sup> and did not modify SOA yield values to account for them.

# 3. RESULTS

**3.1. Overview of D**<sub>5</sub> **SOA Generation.** As mentioned in section 2.1, D<sub>5</sub> was introduced to the OFR at OH<sub>exp</sub> ranging from  $1.1 \times 10^{12}$  to  $8.2 \times 10^{12}$  cm<sup>-3</sup> s and Cl<sub>exp</sub> ranging from  $1.6 \times 10^{10}$  to  $1.6 \times 10^{12}$  cm<sup>-3</sup> s. At the lowest OH<sub>exp</sub> and Cl<sub>exp</sub>, approximately 90 or 94% of D<sub>5</sub> precursor was consumed by reaction with OH or Cl<sup>7</sup> (panels a and e of Figure 1), yet SOA concentrations were negligible. However, a series of C<sub>5</sub>-C<sub>10</sub> OVOCs were detected at these OH and Cl exposures, including  $\sum_{n=0}^{4} C_{5+n} H_{18+2n} O_{9-n} Si_5$  and  $\sum_{n=0}^{3} C_{6+n} H_{22+2n} O_{9-n} Si_5$  compounds as well as  $C_8 H_{22} O_8 Si_5$ ,  $C_9 H_{24} O_7 Si_5$ ,  $C_{10} H_{28} O_7 Si_5$ , and  $C_{10} H_{30} O_6 Si_5$ . Several of these compounds were also detected in D<sub>5</sub> SOA using the VIA (section 3.3.1) and, as such, were likely semivolatile under our experimental conditions. We hypothesize that multigenerational OH/Cl oxidation of these early-generation D<sub>5</sub> + OH/Cl OVOCs was necessary to generate SOA.

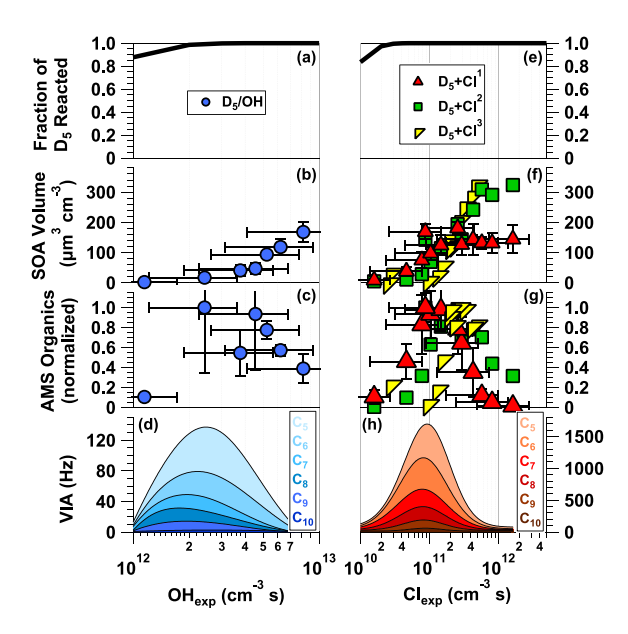


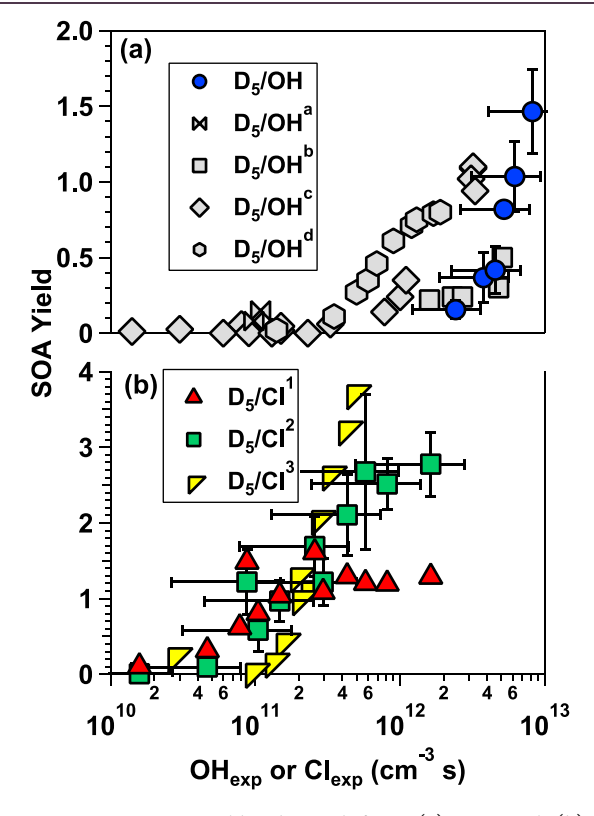
Figure 1. (a) Fraction of D<sub>5</sub> reacted, (b) SOA volume concentration, (c) normalized AMS OA concentration, and (d) VIA C<sub>x</sub>H<sub>y</sub>O<sub>z</sub>Si<sub>5</sub> signals as a function of OH<sub>exp</sub> and (e) fraction of D<sub>5</sub> reacted, (f) SOA volume concentration, (g) normalized AMS OA concentration, and (h) VIA C<sub>x</sub>H<sub>y</sub>O<sub>z</sub>Si<sub>5</sub> signals as a function of Cl<sub>exp</sub> (humid Cl-SOA only). In panels c and g, OA concentrations were normalized to the maximum OA concentration measured for each SOA type. In panels d and h, to reduce the density of data symbols and make the figures easier to read, separate Gaussian or log-normal curves were fit to the summed  $C_5H_vO_zSi_5H^+$ ,  $C_6H_vO_zSi_5H^+$ ,  $C_7H_vO_zSi_5H^+$ ,  $C_8H_vO_zSi_5H^+$ , C<sub>9</sub>H<sub>v</sub>O<sub>z</sub>Si<sub>5</sub>H<sup>+</sup>, and C<sub>10</sub>H<sub>v</sub>O<sub>z</sub>Si<sub>5</sub>H<sup>+</sup> signals. Representative error bars indicate  $\pm 1\sigma$  uncertainty in binned values,  $\pm 50\%$  uncertainty in OH<sub>exp</sub> values, and ±70% uncertainty in Cl<sub>exp</sub> values. Additional figure notes: <sup>1</sup>Cl generated using OFR369-iCl<sub>2</sub> under humid conditions, <sup>2</sup>Cl generated using OFR369-iCl<sub>2</sub> under dry conditions, and <sup>3</sup>Cl generated using OFR254/313-iC<sub>2</sub>Cl<sub>2</sub>O<sub>2</sub> under dry conditions.

Figure 1b shows that the  $D_5$  OH-SOA volume concentration increased monotonically from 2.2 to 168  $\mu$ m³ cm⁻³ as a function of OH<sub>exp</sub>. For humid  $D_5$  Cl-SOA, the SOA volume concentration increased from 8.6 to 144  $\mu$ m³ cm⁻³ as Cl<sub>exp</sub> increased from 1.6 × 10¹0 to 4.3 × 10¹1 cm⁻³ s then was approximately constant up to Cl<sub>exp</sub> = 1.6 × 10¹2 cm⁻³ s (Figure 1f). The volume concentration of dry  $D_5$  Cl-SOA generated using OFR369-iCl₂ or OFR254/313-iC₂Cl₂O₂ increased monotonically from 4.7 to 323  $\mu$ m³ cm⁻³ over a similar range of Cl<sub>exp</sub>. This apparent humidity dependence upon the Cl-SOA yield is discussed further in sections 3.3.1 and 3.3.3. Notably, unlike OH/Cl-SOA generated from other precursors, <sup>25,43</sup> the  $D_5$  SOA volume concentration did not decrease at higher OH<sub>exp</sub> and Cl<sub>exp</sub> as a result of fragmentation reactions that generated higher volatility oxidation products.

In contrast to the continuous increase in OH-SOA and Cl-SOA volume concentrations calculated from the SMPS data, as shown in panels b and f of Figure 1, the organic aerosol (OA) mass concentrations measured by the AMS increased and then decreased as a function of  $OH_{exp}$  and  $CI_{exp}$  (panels c and g of Figure 1). AMS chloride concentrations followed the same trend as AMS OA concentrations (not shown), as did concentrations of  $C_{5-10}H_yO_2Si_5$  signals detected in OH-SOA and Cl-SOA with the VIA (panels d and h of Figure 1 and Figure S4 of the Supporting Information). Because both AMS and VIA heat the SOA particles to detect them in the gas phase

(whereas the SMPS does not), this suggests that the SOA became refractory as a function of oxidative aging. Additional observations supporting this hypothesis are presented in sections 3.3.1 and 3.3.3.

**3.2. Yields of D** $_5$  OH-SOA and Cl-SOA. Panels a and b of Figure 2 show mass yields of D $_5$  OH-SOA and Cl-SOA as a



**Figure 2.** SOA mass yields obtained from (a) OH and (b) Cl oxidation of  $D_5$  as a function of  $OH_{exp}$  and  $Cl_{exp}$ . Different y-axis scales are used in each subpanel. Representative error bars indicate  $\pm 1\sigma$  uncertainty in binned SOA yield values,  $\pm 50\%$  uncertainty in  $OH_{exp}$  exposure values, and  $\pm 70\%$  uncertainty in  $OH_{exp}$  exposure values. Additional figure notes:  $^aWu$  and Johnston,  $^{2.2b}$ Janechek et al.,  $^{14c}$ Charan et al.,  $^{16d}$ Han et al.,  $^{441}$ Cl generated using OFR369-iCl<sub>2</sub> under humid conditions,  $^2$ Cl generated using OFR369-iCl<sub>2</sub> under dry conditions, and  $^3$ Cl generated using OFR254/313-iC<sub>2</sub>Cl<sub>2</sub>O<sub>2</sub> under dry conditions.

function of  $OH_{exp}$  and  $Cl_{exp}$ . Results obtained from OH oxidation of  $D_5$  in previous studies are shown for reference in Figure 2a. Here, the  $D_5$  OH-SOA yield increased monotonically from 0.02 to 1.5 as a function of  $OH_{exp}$  (Figure 2a). These values agree within  $\pm 35\%$  of those obtained by Janechek et al. And Charan et al. between  $OH_{exp} = 2.3 \times 10^{12}$  and 5.2  $\times 10^{12}$  cm<sup>-3</sup> s and encompass the range of yields (0.02–0.80) obtained by Han et al. Between  $OH_{exp} = 1.4 \times 10^{11}$  and 1.9  $\times 10^{12}$  cm<sup>-3</sup> s. The OH-SOA yield nearly doubled from 0.82 to 1.5 between  $OH_{exp} = 5.2 \times 10^{12}$  and 8.2  $\times 10^{12}$  cm<sup>-3</sup> s. OH-SOA yields between 0.08 and 0.15 were measured by Wu and Johnston at lower  $OH_{exp}$  values ( $\approx 10^{11}$  cm<sup>-3</sup> s) than were used in this study.

Figure 2b shows that yields of  $D_5$  Cl-SOA increased from <0.10 at  $Cl_{exp} = 1.6 \times 10^{10}$  cm<sup>-3</sup> s to 1.3 at  $Cl_{exp} = 2 \times 10^{11}$  to  $3 \times 10^{11}$  cm<sup>-3</sup> s in both dry and humid conditions. At higher  $Cl_{exp}$ , yields of Cl-SOA remained approximately constant at 1.3 under humid conditions, whereas yields of Cl-SOA generated in dry conditions increased to 2.7 (OFR369-iCl<sub>2</sub>) and 3.8

(OFR254-iC<sub>2</sub>Cl<sub>2</sub>O<sub>2</sub>) at the highest Cl<sub>exp</sub>. Assuming an upperlimit D<sub>5</sub> SOA yield value of approximately 1.8 via generation of hypothetical oxidation product  $C_{10}H_{10}O_{25}Si_5$  (MW = 670 g  $\text{mol}^{-1}$ ) via  $\text{CH}_3 \rightarrow \text{C(O)OH}$  functionalization reactions, Cl-SOA yield values ranging from 2.7 to 3.8 are chemically implausible. Because similar maximum yields were obtained with OFR369-iCl<sub>2</sub> and OFR254/313-iC<sub>2</sub>Cl<sub>2</sub>O<sub>2</sub> methods, this suggests that organic chlorides, which could, in principle, be generated as artifacts following reactive uptake of Cl<sub>2</sub> to the SOA, did not contribute a significant additional SOA yield. Järvinen et al. 45 generated non-spherical  $\alpha$ -pinene SOA particle aggregates following coauglation of highly viscous nucleated (spherical) particles at low RH.<sup>45</sup> We hypothesize that a similar phenomenon may have occurred for dry D5 Cl-SOA particles generated at the highest Clexp used here. If so, this process would reduce the density of aggregates relative to the calculated material density (which implicitly assumes spherical particle morphology as applied here), thereby biasing the calculated dry Cl-SOA yield values high. Figure S1 of the Supporting Information shows that the mean particle mobility diameter  $(D_m)$  of humid Cl-SOA decreased while  $D_m$  of dry Cl-SOA generated via OFR369-iCl<sub>2</sub> and OFR254/313iC<sub>2</sub>Cl<sub>2</sub>O<sub>2</sub> increased as a function of Cl<sub>exp</sub>. Because particle density is proportional to the ratio of the particle aerodynamic diameter  $(D_a)$  and mobility diameter, 46 hypothetically, constant  $D_a$  coupled with decreasing  $D_m$  (humid Cl-SOA) or increasing  $D_{\rm m}$  (dry Cl-SOA) would support our hypothesis. However, in the absence of available  $D_a$  measurements in these studies, definitive conclusions about changes in humiditydependent particle density are not possible.

3.3. Chemical Composition of D<sub>5</sub> OH-SOA and Cl-SOA. 3.3.1. AMS Spectra of D<sub>5</sub> OH-SOA and Cl-SOA. Figure 3

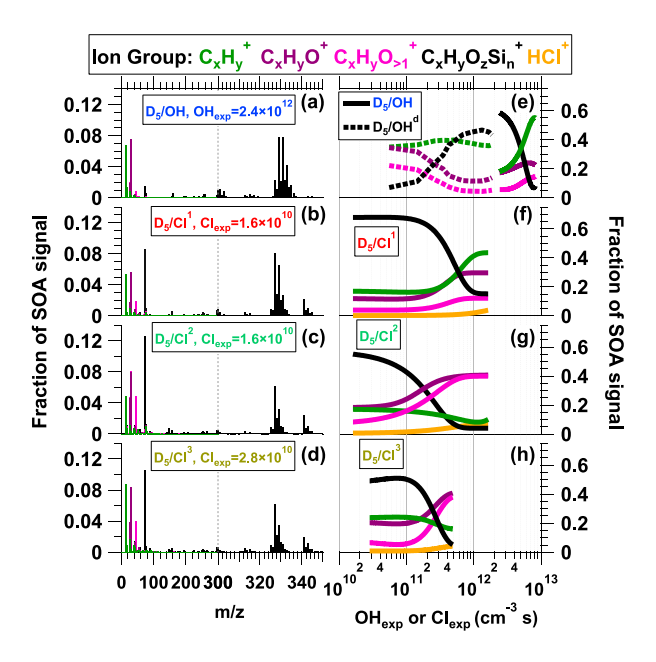


**Figure 3.** AMS spectra of SOA generated from (a and e) OH oxidation of  $D_5$ , (b and f) Cl oxidation of  $D_5$  under humid conditions, and (c, d, g, and h) Cl oxidation of  $D_5$  under dry conditions. OH<sub>exp</sub> and Cl<sub>exp</sub> values listed in panels a–d are in units of cm<sup>-3</sup> s. Additional figure notes:  $^1$ Cl generated using OFR369-iCl<sub>2</sub> under humid conditions,  $^2$ Cl generated using OFR369-iCl<sub>2</sub> under dry conditions,  $^3$ Cl generated using OFR254/313-iC<sub>2</sub>Cl<sub>2</sub>O<sub>2</sub> under dry conditions, and  $^4$ Han et al.  $^{44}$ 

shows AMS spectra of SOA generated from the OH and Cl oxidation of  $D_5$  at  $OH_{exp} = 2.4 \times 10^{12}$  cm<sup>-3</sup> s and  $Cl_{exp} = 1.6 \times 10^{12}$ 10<sup>10</sup> cm<sup>-3</sup> s, respectively. At these exposures, as a result of the relative reaction rates of  $D_5$  + OH and  $D_5$  +  $Cl_7$  we anticipate that the extent of OH and Cl oxidation of D<sub>5</sub> and/or its oxidation products is the same within ≈30% uncertainty. Both D<sub>5</sub> OH-SOA and Cl-SOA spectra were dominated by  $C_x H_v O_z Si_n^+$  ion groups, which contributed 61 and 69% of the total OH-SOA and Cl-SOA signal, respectively (panels e and f of Figure 3). Within this ion group, m/z 329  $(C_4H_{13}O_8Si_5^+)$  and m/z 331  $(C_4H_{11}O_{10}Si_4^+)$  were the largest signals in the OH-SOA spectrum, whereas m/z 73 (C<sub>3</sub>H<sub>9</sub>Si<sup>+</sup>), m/z 327 (C<sub>5</sub>H<sub>15</sub>O<sub>7</sub>Si<sub>5</sub><sup>+</sup>), and C<sub>4</sub>H<sub>13</sub>O<sub>8</sub>Si<sub>5</sub><sup>+</sup> were the largest signals in the Cl-SOA spectra and an AMS spectra of D<sub>5</sub> OH-SOA measured elsewhere. Han et al. 44 assigned  $C_{12}H_{11}O_2Si_5^+$ ,  $C_9H_9O_8Si_5^+$ , and  $C_5H_{15}O_9Si_4^+$  to signals at m/z 327, 329, and 331 in their AMS spectrum of D<sub>5</sub> OH-SOA. These formulas can also explain our signals at those nominal m/z values but require significantly more complex fragmentation in the AMS than our proposed assignments. Other signals that were present at large abundances in both OH-SOA and Cl-SOA spectra include m/z 15 (CH<sub>3</sub><sup>+</sup>), which corresponds to methyl groups that were bonded to Si atoms, m/z 29 (CHO<sup>+</sup>), a marker for alcohols,  $^{38}$  and m/z 44 (CO<sub>2</sub>+), a marker for organic acids<sup>48</sup> and potentially also formate esters.<sup>49,50</sup>

Figure S2 of the Supporting Information shows AMS  $C_x H_v O_z Si_n^+$  signals that were detected in  $D_5$  OH-SOA and Cl-SOA spectra above m/z 350. In general, AMS signals in this range of higher m/z are less common as a result of high-energy electron impact ionization of 70 eV and flash vaporization at T = 600 °C that result in thermal decomposition and fragmentation of the analyte molecules; their presence here underscores the stability of siloxanes that undergo both processes. The most prominent feature of the OH-SOA spectrum (Figure S2a of the Supporting Information) was a cluster of ion signals observed at m/z 639-671, whereas several distinct ion clusters were detected in the Cl-SOA spectrum between m/z 579-587, 595-602, 637-647, 653-661, and 669-675 (Figure S2b of the Supporting Information). Additional ion clusters were detected in both spectra at m/z 895–902, 909–916, 923–930, 955–962, 969–976, and 983-990. Unambiguous assignment of chemical formulas to the ion signals shown in Figure S2 of the Supporting Information is difficult as a result of the limited range of the AMS m/z calibration ( $m/z \le 355$ ,  $C_9H_{27}O_5Si_5^+$ ); however, the relative abundances of <sup>29</sup>Si and <sup>30</sup>Si isotopes suggest that they contain 10 Si atoms. Thus, at these OH<sub>exp</sub> and Cl<sub>exp</sub> values, dimers were present in D5 SOA, as observed in earlier studies. 10,22 The different fragmentation patterns shown in panels a and b of Figure S2 of the Supporting Information reflect differences in the chemical composition of dimers that were present in D<sub>5</sub> OH-SOA and Cl-SOA.

Panels e—h of Figure 3 plot fractional contributions of the  $C_xH_y^+$ ,  $C_xH_yO_1^+$ ,  $C_xH_yO_{\geq 1}^+$ ,  $C_xH_yO_zSi_n^+$ , and  $Cl^+ + HCl^+$  ion groups  $(f_{C_xH_y^+}, f_{C_xH_yO_1^+}, f_{C_xH_yO_{\geq 1}^+}, f_{C_xH_ySi_zO_n^+}, \text{and } f_{HCl^+})$  present in  $D_5$  OH/Cl-SOA as a function of oxidant exposure. Here,  $f_{HCl^+}$  was used as a marker for condensed-phase organic chlorides (ROCl),  $^{25,51,52}$  assuming that uptake of gas-phase HCl to the SOA was negligible. Minimal signals were observed at other  $C_xH_yO_zCl^+$ -containing ions. In all cases,  $f_{C_xH_yO_zSi_n^+}$  decreased monotonically over the range of  $OH_{exp}$  and  $Cl_{exp}$  used here. In a different study,  $^{44}f_{C_xH_xO_xSi_n^+}$  of  $D_5$  OH-SOA increased from

0.07 to 0.47 as  $OH_{exp}$  was increased from 1.5  $\times$   $10^{11}$  to 1.3  $\times$   $10^{12}$  cm<sup>-3</sup> s before it began to decrease. Taken together with our results, this suggests that the AMS  $C_x H_y O_z Si_n^+$  ion group represents a class of intermediate oxidation products whose consumption following reaction with OH/Cl generates extremely low-volatility oxidation products that contribute to higher SOA yields observed at higher  $OH_{exp}$  or  $Cl_{exp}$ .

For OH-SOA and humid Cl-SOA,  $f_{C_xH_y^*}$ ,  $f_{C_xH_yO_1^*}$ , and  $f_{C_xH_yO_{\ge 1}^*}$  increased, whereas for dry Cl-SOA,  $f_{C_xH_y^*}$  decreased while  $f_{C_xH_yO_1^*}$  and  $f_{C_xH_yO_{\ge 1}^*}$  increased. The maximum  $f_{C_xH_yO_1^*}$  and  $f_{C_xH_yO_{\ge 1}^*}$  values were lower in humid Cl-SOA (0.12) than in dry Cl-SOA (0.38–0.40). Despite the lack of double bonds in  $D_5$  for direct Cl or Cl<sub>2</sub> addition, evidence of ROCl formation was observed in Cl-SOA:  $f_{HCl^*}$  followed the same trend as  $f_{C_xH_yO_{\ge 1}^*}$  with increasing Cl<sub>exp</sub> as observed in other Cl-SOA types. One possible source of ROCl may have been the reaction  $RO_2 + Cl \rightarrow RO + ClO$  followed by the reaction  $RO_2 + Cl \rightarrow ROCl + O_2^{53,54}$  where  $RO_2$  represents organic peroxy radicals derived from Cl oxidation of  $D_5$  and/or its oxidation products and RO represents alkoxy radicals.

3.3.2. VIA Spectra of  $D_5$  OH-SOA and CI-SOA. Figure 4a shows a VIA spectrum of SOA generated from the OH

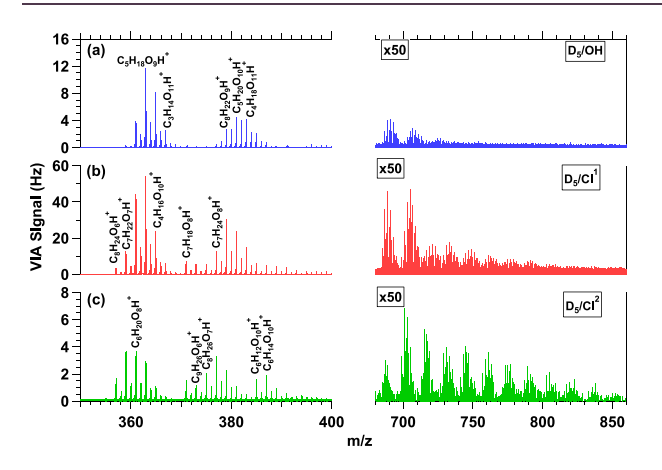


**Figure 4.** VIA spectra of SOA generated from (a) OH oxidation of  $D_5$  (OH<sub>exp</sub> =  $2.4 \times 10^{12}$  cm<sup>3</sup> s<sup>-1</sup>), (b) Cl oxidation of  $D_5$  under humid conditions (Cl<sub>exp</sub> =  $4.6 \times 10^{10}$  cm<sup>3</sup> s<sup>-1</sup>), and (c) Cl oxidation of  $D_5$  under dry conditions (Cl<sub>exp</sub> =  $4.6 \times 10^{10}$  cm<sup>3</sup> s<sup>-1</sup>). Signals shown are unmodified (M + H)<sup>+</sup> formulas. Additional figure notes: <sup>1</sup>Cl generated using OFR369-iCl<sub>2</sub> under humid conditions and <sup>2</sup>Cl generated using OFR369-iCl<sub>2</sub> under dry conditions.

oxidation of  $D_5$  at the same  $OH_{exp}$  as the AMS spectrum shown in Figure 3a. Here, signals between m/z 350–400 and 660–860 are shown; full product spectra are shown on a logarithmic scale in Figure S3a of the Supporting Information. A list of molecular formulas of major  $C_xH_yO_zSi_5$  compounds detected with the VIA is shown in Table S1 of the Supporting Information. The OH-SOA spectrum shown in Figure 4a was dominated by two clusters of signals between m/z 361–369 and 377–387. The ions at m/z 363 ( $C_5H_{18}O_9Si_5H^+$ , detected previously in  $D_5$  SOA<sup>22</sup>) and m/z 365 ( $C_4H_{16}O_{10}Si_5H^+$ ) were the largest signals in the OH-SOA spectrum. We hypothesize that  $C_5H_{18}O_9Si_5$  and  $C_4H_{16}O_{10}Si_5$  are carbonyl siloxanols generated following three and four  $CH_3 \rightarrow OH$  fragmentation reactions, respectively,  $^{22,50}$  plus the replacement of two adjacent methyl groups with a carbonyl  $[SiO_2(CH_3)_2 \rightarrow$ 

 $Si(O)O_2$ ]. Similarly, carbonyl siloxanols detected at m/z 361 ( $C_6H_{20}O_8Si_5H^+$ ) and m/z 367 ( $C_3H_{14}O_{11}Si_5H^+$ ) were likely generated by two and five  $CH_3 \rightarrow OH$  fragmentation reactions plus one  $SiO_2(CH_3)_2 \rightarrow Si(O)O_2$  fragmentation reaction. Other significant product ions with 2 or fewer DBEs were detected at m/z 377, 379, 381, and 383. These signals represent siloxanols that were generated by three to six  $CH_3 \rightarrow OH$  fragmentation reactions.

Panels b and c of Figure 4 show VIA spectra of SOA generated from the Cl oxidation of  $D_5$  at  $Cl_{exp} = 4.6 \times 10^{10}$ cm<sup>-3</sup> s under dry and humid conditions (comparison spectra were not available at both conditions at  $Cl_{exp} = 1.6 \times 10^{10}$  cm<sup>-3</sup> s). Many of the same ions detected in Cl-SOA spectra were also detected in the OH-SOA spectrum. However, signals at m/z 357 (C<sub>8</sub>H<sub>24</sub>O<sub>6</sub>Si<sub>5</sub>H<sup>+</sup>), 359 (C<sub>7</sub>H<sub>22</sub>O<sub>7</sub>Si<sub>5</sub>H<sup>+</sup>), and 361  $(C_6H_{20}O_8Si_5H^+)$ , which were generated by zero to two  $CH_3 \rightarrow$ OH fragmentation reactions plus one  $SiO_2(CH_3)_2 \rightarrow Si(O)O_2$ fragmentation reaction, were enhanced in Cl-SOA relative to OH-SOA, as were signals at m/z 373 (C<sub>9</sub>H<sub>28</sub>O<sub>6</sub>Si<sub>5</sub>H<sup>+</sup>), 375  $(C_8H_{26}O_7Si_5H^+)$ , 377  $(C_7H_{24}O_8Si_5H^+)$ , and 379  $(C_6H_{22}O_9Si_5H^+)$ . Further,  $C_8H_{24}O_6Si_5H^+$  and  $C_7H_{22}O_7Si_5H^+$ as well as ions at m/z 385 and 387 that contained  $\geq$ 3 DBEs were enhanced in the dry Cl-SOA spectrum relative to the humid Cl-SOA spectrum.

As was the case with AMS spectra, another notable difference between VIA spectra of D<sub>5</sub> OH-SOA and Cl-SOA was the relative abundance and composition of signals between m/z 660 and 860 that represent  $C_xH_yO_zSi_{10}$  dimer oxidation products. In OH-SOA, three clusters of signals between m/z687-697, 703-715, and 721-733 were detected, whereas at least eight clusters were detected in Cl-SOA. While a detailed discussion of the  $C_xH_vO_zSi_{10}$  composition of each SOA type is beyond the scope of this analysis, we briefly note that the 37 C<sub>x</sub>H<sub>y</sub>O<sub>z</sub>Si<sub>10</sub> species identified in D<sub>5</sub> OH-SOA by Wu and Johnston were detected in our VIA OH/Cl-SOA spectra along with numerous additional compounds. Additionally, Figure 4 shows that the relative yield of dimers was lowest in D<sub>5</sub> OH-SOA and highest in dry Cl-SOA. Because reaction with OH and/or hydroperoxyl radicals (HO<sub>2</sub>) was the dominant RO<sub>2</sub> loss pathway in OH-SOA experiments (section 4), formation of dimers via RO<sub>2</sub> + RO<sub>2</sub> reactions was suppressed in OH-SOA relative to Cl-SOA. As will be discussed in section 4, H<sub>2</sub>O also appears to suppress dimer formation to some extent in humid Cl-SOA relative to dry Cl-SOA.

A comparison of the AMS and VIA spectra shown in Figures 3 and 4 suggests that there was significant overlap between the major C<sub>x</sub>H<sub>y</sub>O<sub>z</sub>Si<sub>5</sub><sup>+</sup> signals detected by both techniques at the lowest oxidant exposures that were used  $(OH_{exp} = 2.4 \times 10^{12})$ and  $Cl_{exp} = 1.6 \times 10^{10}$  to  $4.6 \times 10^{10}$  cm<sup>-3</sup> s). For example,  $C_5H_{18}O_9Si_5$  was detected at  $C_5H_{18}O_9Si_5H^+$  in the VIA, and we hypothesize that the same compound fragmented into  $C_4H_{13}Si_5O_8^+ + CH_3^+$  ions in the AMS along with  $H_2O$ elimination. Similarly, we hypothesize that C<sub>6</sub>H<sub>20</sub>O<sub>8</sub>Si<sub>5</sub> was detected at  $C_6H_{20}O_8Si_5H^+$  in the VIA and  $C_5H_{15}O_7Si_5^+$  + CH<sub>3</sub><sup>+</sup> in the AMS, again accompanied by H<sub>2</sub>O elimination. While a more extensive series of dimers was observed in both AMS and VIA spectra of Cl-SOA compared to OH-SOA (Figure S2 of the Supporting Information and Figure 4), a direct comparison between  $C_xH_vO_zSi_{10}^+$  signals detected in the AMS and VIA spectra was not possible. This is presumably because dimer oxidation products experienced more complex fragmentation/decomposition in the AMS than monomers. Additionally, there was less overlap between AMS and VIA

spectra obtained at higher  $OH_{exp}$  and  $Cl_{exp}$  than in those shown in Figures 3 and 4. Specifically, later-generation carboxylic acids/formate ester oxidation products were more efficiently detected by the AMS than by the VIA as a result of the lower selectivity of  $H_3O^+$  reagent toward highly oxidized compounds. Implications of the different instrument responses to early- versus later-generation  $D_5$  oxidation products are discussed in the following section, where we examine changes in the elemental composition of  $D_5$  SOA to provide information about the nature of associated oxidative aging pathways. So

3.3.3. Elemental Composition of OH-SOA and CI-SOA. Diagrams that show C/Si as a function of O/Si can be used to track  $CH_3 \rightarrow CH_2OH (\Delta C/Si/\Delta O/Si = 0)$  and  $CH_3 \rightarrow OH$  $(\Delta C/Si/\Delta O/Si = -1)$  functionalization and fragmentation reactions in D<sub>5</sub> SOA, <sup>10</sup> where O/Si may, in principle, increase from 0.5 to 4 with an accompanying decrease in C/Si from 2 to 0 following conversion of  $D_5$  to orthosilicate (SiO<sub>4</sub><sup>4-</sup>) as a hypothetical oxidation end product. Ensemble C/Si and O/Si values extracted from AMS spectra of D<sub>5</sub> OH-SOA and Cl-SOA are shown in Figure S5 of the Supporting Information. C/Si and O/Si of the least oxidized D<sub>5</sub> OH/Cl-SOA ranged from 2.5 to 3.5 and from 1.8 to 2.9, respectively. While these C/Si values are larger than C/Si of D<sub>5</sub>, they may be plausible within the uncertainty of unknown AMS sensitivity to Si. However, Figure S5 of the Supporting Information shows that C/Si and O/Si both increased to maximum values ranging from 22 to 60 and from 10 to 67, respectively, as a function of OH<sub>exp</sub> or Cl<sub>exp</sub>. While loss of particulate Si is possible, <sup>10,44</sup> it seems unlikely that it can occur to the extent that would be necessary to explain these observations. There are two alternative explanations for these results. First, conversion of particulate Si to refractory aerosol with aging may have decreased its volatility relative to the carbon-containing functional groups attached to the siloxane backbone. An accompanying change in thermal decomposition/fragmentation mechanisms may have resulted in less volatile Si species producing lower Si/C ratios that higher volatility species. This bias would not be accounted for in the elemental analysis method used here. Second, early-generation oxidation products that generated  $C_x H_v O_z Si_n^+$  signals in the AMS may have been converted to later-generation oxidation products in the OFR that preferentially generated Si<sup>+</sup> (m/z 27.97) and/or SiO<sup>+</sup> (m/zz 43.97) signals, which were difficult to isolate from  $N_2^+$  and  $CO_2^+$  signals at the same nominal m/z 28 and 44 values. We estimated upper limit contributions of Si<sup>+</sup> and SiO<sup>+</sup> by adding them to the AMS peak list and then recalculating C/Si and O/ Si for dry Cl-SOA, which had the highest O/Si of all D<sub>5</sub> SOA types examined here. While this analysis yielded maximum C/ Si and O/Si values of 4.2 and 4.8 (down from C/Si = 60 and O/Si = 67 without fitting  $Si^+$  and  $SiO^+$ ), which may be plausible within uncertainties, it did not significantly change the overall trends of C/Si and O/Si as a function of oxidant exposure. Because the analysis of C/Si and O/Si values was inconclusive (perhaps as a result of inefficient detection of Si, SiO, or RSiO compounds), we instead constructed a Van Krevelen diagram that showed H/C as a function of O/C to examine oxidative aging pathways of the methyl groups present in D<sub>5</sub> SOA.

Ensemble H/C and O/C values extracted from AMS spectra of  $D_5$  SOA are shown in Figure 5. The atomic O/C and H/C values of  $D_5$  as well as trendlines for  $CH_3 \rightarrow CH_2OH$ ,  $CH_3 \rightarrow OH$ ,  $CH_3 \rightarrow CH_2OH$ ,  $CH_3 \rightarrow COOOH$  or OCOOOH, and

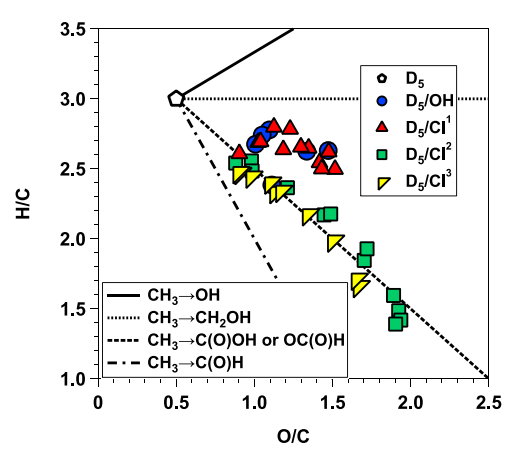


**Figure 5.** Van Krevelen diagrams showing the H/C ratio as a function of the O/C ratio for  $D_5$  OH-SOA and Cl-SOA. Additional figure notes:  $^1\text{Cl}$  generated using OFR369-iCl $_2$  under humid conditions,  $^2\text{Cl}$  generated using OFR369-iCl $_2$  under dry conditions, and  $^3\text{Cl}$  generated using OFR254/313-iC $_2\text{Cl}_2\text{O}_2$ .

 ${
m CH_3} 
ightharpoonup {
m C(O)} {
m H}$  functionalization/fragmentation reactions are shown for reference. These trendlines have Van Krevelen slopes ( $\Delta {
m H/C/\Delta O/C}$ ) of 0.67, 0, -1, and -2, respectively. Functionalization reactions that convert methyl groups to peroxide groups may also have occurred, with a corresponding Van Krevelen slope of 0. Because peroxides are known to fragment in the Vocus PTR,  $^{57}$  we could not unambiguously identify them in our measurements; thus, they are not discussed further here.

Figure 5 shows that  $D_5$  OH-SOA had O/C and H/C ranging from 1.0 to 1.5 and from 2.6 to 2.8, respectively. Dry Cl-SOA had O/C = 0.88-1.9 and H/C = 1.4-2.5, whereas humid Cl-SOA had O/C = 0.90-1.5 and H/C = 2.5-2.8. In OH-SOA and humid Cl-SOA, H/C increased from 2.6 to 2.8 as O/C increased from 1.0 to 1.2 before H/C decreased to 2.5 at O/C = 1.5. Corresponding average Van Krevelen slopes were -0.27(OH-SOA) and -0.11 (humid Cl-SOA). This overall trend was consistent with expected CH<sub>3</sub> → OH and/or CH<sub>3</sub> → CH<sub>2</sub>OH reactions at lower OH<sub>exp</sub> or Cl<sub>exp</sub>, <sup>10,50</sup> followed by the formation of carbonyl, carboxylic acid, and/or formate ester functional groups at higher oxidant exposures. On the other hand, H/C of dry Cl-SOA decreased continuously from 2.5 to 1.4 with increasing O/C, with an average Van Krevelen slope ranging from -1.03 (OFR254/313-iC<sub>2</sub>Cl<sub>2</sub>O<sub>2</sub>) to -1.07(OFR369-iCl<sub>2</sub>). This trend, along with the accompanying increase in AMS  $CO_2^+$  signal, suggests that  $CH_3 \rightarrow C(O)OH$ and/or  $CH_3 \rightarrow OC(O)H$  reactions were significant in dry Cl-SOA.

Table S1 of the Supporting Information lists 24 major  $C_xH_yO_zSi_5$  tracers that were detected with the VIA and presented in Figure 4. Compounds with ≤2 DBEs were generated via  $CH_3 \rightarrow OH$  reactions, including the series of  $C_9H_{28}O_6Si_5$  through  $C_4H_{18}O_{11}Si_5$  siloxanols and  $C_8H_{24}O_6Si_5$  through  $C_3H_{14}O_{11}Si_5$  carbonyl siloxanols. These compounds have atomic O/C values ranging from 0.67 to 3.67, which more than span the range of ensemble O/C values extracted from AMS spectra. However, their corresponding H/C values (3.0–4.7) were higher than AMS-derived H/C values, and this divergence increased with increasing O/C. A series of  $C_{6-8}H_{12-20}O_{7-10}Si_5$  compounds measured with VIA that contain ≥ 2 DBEs more closely tracked ensemble O/C and H/C values of  $D_5$  OH/Cl-SOA. We hypothesize that these

compounds represent dehydration/decarboxylation products of thermally labile species in the VIA whose behavior in the instrument is not yet known. Thus, we cannot yet make definitive conclusions about their composition or contributions to  $D_5$  SOA at higher  $OH_{exp}$  and  $Cl_{exp}$ .

# 4. DISCUSSION

Differences in D<sub>5</sub> OH-SOA and Cl-SOA composition that are summarized in Figures 3-5 are associated with differences in the fate of RO<sub>2</sub> derived from OH or Cl oxidation of D<sub>5</sub> and its early-generation oxidation products. To investigate the fate of RO<sub>2</sub> in these studies, we calculated the fractional oxidative loss of a generic siloxy  $RO_2$  ( $F_{RO_2}$ ) generated from the OH or Cl oxidation of 12 ppbv  $D_5$  as a function of  $OH_{\text{exp}}$  or  $Cl_{\text{exp}}$  using the KinSim chemical kinetic solver. Se Kinetic data used in these calculations 7,30,59-64 are provided in Table S2 of the Supporting Information; the corresponding reactions were added to the KinSim mechanism published previously by our group. 25 Here, we assumed RO<sub>2</sub> reacted with OH, HO<sub>2</sub>, Cl, ClO, RO2, and/or underwent autoxidation via sequential isomerization and O<sub>2</sub> addition. Alton and Browne<sup>50</sup> proposed a humidity-dependent mechanism for the gas-phase OH/Cl oxidation of D<sub>3</sub> in which RO that was generated following RO<sub>2</sub> isomerization reacted with H2O, generating a silanol and OH as co-products. To evaluate the potential effect of this reaction on the RO<sub>2</sub> fate, we set the RO +  $H_2O$  rate coefficient to 4  $\times$  $10^{-12}$  cm<sup>3</sup> s<sup>-1</sup> to make this reaction proceed at the same rate as RO2 isomerization/autoxidation reactions and then calculated  $F_{RO_2}$  in  $D_5/Cl$  experiments with and without this reaction enabled in the model.

In D<sub>5</sub>/OH studies, the main RO<sub>2</sub> loss pathways were RO<sub>2</sub> +  $HO_2$  and  $RO_2$  + OH reactions:  $F_{RO_2+HO_2}$  decreased from 0.36 to 0.17 and  $F_{\rm RO_2+OH}$  decreased from 0.63 to 0.83 as a function of OH<sub>exp</sub> (Figure 6a). RO<sub>2</sub> consumption as a result of isomerization/autoxidation and reaction with other RO2 were minor (<1% of total RO<sub>2</sub> loss). In  $D_5/Cl$  studies, the RO<sub>2</sub> fate was more complex. With the RO +  $H_2O$  reaction enabled (e.g., in humid conditions), as a function of  $Cl_{exp}$ ,  $F_{RO_2+RO_2}$  decreased from 0.11 to 0.003,  $F_{\rm RO_2}$  as a result of isomerization/ autoxidation decreased from 0.15 to 0.002,  $F_{RO,+Cl}$  increased from 0.24 to 0.33, and  $F_{RO_2+CIO}$  increased from 0.21 to 0.32 (Figure 6b). As a result of OH formation via the RO + H<sub>2</sub>O reaction,  $F_{\mathrm{RO}_2+\mathrm{OH}}$  was likewise significant and increased from 0.29 to 0.35 as a function of  $Cl_{exp}$ . Under dry conditions, at low  $Cl_{exp}$ ,  $F_{RO_2+RO_2} = 0.24$ ,  $F_{RO_2+Cl} = 0.30$ ,  $F_{RO_2+ClO} = 0.27$ , and  $F_{RO_2} = 0.27$ = 0.19 as a result of isomerization/autoxidation were all higher than under humid conditions (Figure 6c). As expected, these trends are qualitatively consistent with the higher yields of dimers and ROCl that were observed in dry Cl-SOA relative to humid Cl-SOA and OH-SOA (Figures 3 and 4). Likewise, the higher SOA oxidation state of dry Cl-SOA was associated with higher yields of carboxylic acids/formate esters formed via isomerization/autoxidation and/or RO<sub>2</sub> + Cl/ClO reactions (Figures 3 and 5). As was observed for RO<sub>2</sub> generated in humid  $D_5/Cl$  studies,  $F_{RO_2+RO_2}$  and  $F_{RO_2}$  as a result of isomerization/autoxidation approached zero at high  $\text{Cl}_{\text{exp}}$ , where  $F_{RO_2+Cl}$  and  $F_{RO_2+ClO}$  were the only important RO<sub>2</sub> loss pathways.

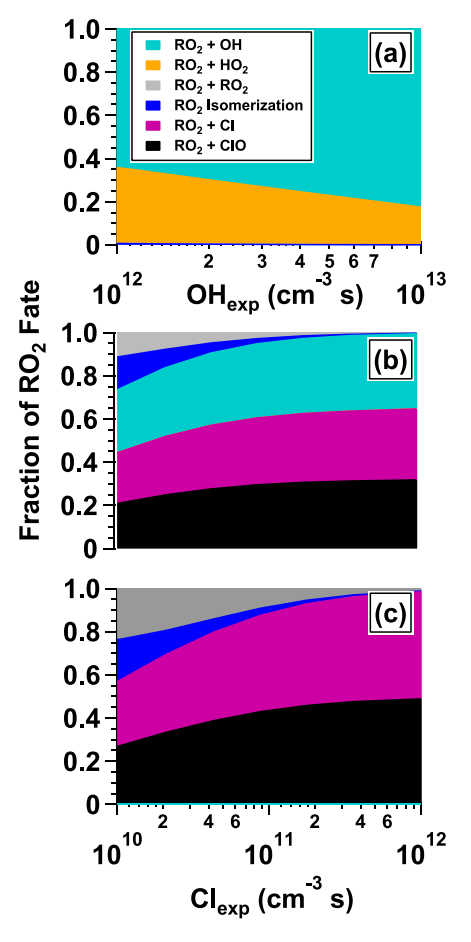


**Figure 6.** Fate of organic peroxy radicals  $(RO_2)$  generated from (a) OH, (b) Cl (humid), and (c) Cl (dry) oxidation of  $D_5$  as a function of  $OH_{exp}$  or  $Cl_{exp}$ . Reactions and kinetic rate coefficients used in these calculations are provided in Table S2 of the Supporting Information.

# 5. CONCLUSION

In this study, we characterized the yields, mass spectra, and elemental composition of SOA generated from the OH and Cl oxidation of D<sub>5</sub>. D<sub>5</sub> OH-SOA and humid Cl-SOA had the highest degree of similarity, and dry Cl-SOA was the most unique; these similarities and differences are most closely associated with the overall RO2 fate in each SOA type. Results presented in section 3.2 indicate the high SOA formation potential of D<sub>5</sub>: SOA yields of OH-SOA and humid Cl-SOA approached 1.5 and 1.3 at the highest OH<sub>exp</sub> and Cl<sub>exp</sub> values that were used. These SOA yields are comparable to or greater than yields of SOA obtained from OH/Cl oxidation of alkanes studied previously.  $^{25,52,65-69}$  While CH<sub>3</sub>  $\rightarrow$  OH fragmentation reactions resulting in carbon loss occurred, the fact that the majority of oxidation products detected by the AMS and the VIA contained 5 or 10 Si atoms suggests that the cyclic Si-O backbone of D<sub>5</sub> was mostly retained. Therefore, the average volatility of the oxidation products continued to decrease as remaining C atoms experienced fragmentation reactions, to the point that the SOA became more refractory at the highest oxidant exposures.

Multiple days of equivalent atmospheric OH exposure were required to achieve significant OH-SOA formation. However, most of the exposure time that was required was associated with the long OH lifetime of  $D_5$ . As noted throughout this paper, lower Cl concentrations were required to generate SOA

because the  $D_5$  + Cl reaction rate is nearly 2 orders of magnitude faster than that of  $D_5$  + OH.<sup>7</sup> Because estimated atmospheric Cl concentrations vary between  $10^3$  and  $10^5$  cm<sup>-3</sup>, the corresponding atmospheric Cl-SOA formation potential of  $D_5$  ranges from insignificant to potentially important on time scales of a day or so in source regions influenced by active chlorine chemistry.<sup>32</sup> Indoor Cl concentrations that reach  $10^5$  to  $10^8$  cm<sup>-3</sup> following bleach cleaning or disinfection activities<sup>19,70</sup> may also be sufficient to achieve  $D_5$  Cl-SOA formation in occupied spaces with low air exchange rates.

Our results indicate that SOA generated from the OH/Cl oxidation of D<sub>5</sub> and potentially other cVMS pose several unique challenges for the AMS that warrant further investigation in future studies. First, the refractory nature of D<sub>5</sub> SOA suggests that only a fraction of it is detected at typical AMS operating conditions. To improve AMS detection of cVMS SOA, future studies should investigate the effect of increasing the vaporizer temperature from the nominal 600 °C set point that is commonly used to ~800 °C. 71,72 Second, the AMS ionization efficiency of Si has not been measured directly because inorganic Si standards, such as silicon dioxide and silicic acid, are refractory. Measurements of cVMS SOA (section 3.3.3 and Figure S5 of the Supporting Information) and  $D_{15}$ – $D_{18}$  siloxanes<sup>73</sup> suggest that the AMS sensitivities to organosilicon and non-Si-containing organic compounds are within a factor of 2 of each other. In principle, to provide better constraints, non-refractory inorganic Si aerosol standards would be required. Third, the relatively high thermal stability of D<sub>5</sub> SOA results in significant formation of product ions at m/z > 350, yet there are few, if any, instrument background signals in this m/z range that can be used to constrain ion formula assignments. Simultaneous measurement of high-molecular-weight aerosol standards, such as Fomblin pump oils,<sup>74</sup> may be required for this purpose.

# ASSOCIATED CONTENT

#### Supporting Information

The Supporting Information is available free of charge at https://pubs.acs.org/doi/10.1021/acsearthspace-chem.2c00304.

AMS spectra of  $D_5$  SOA between m/z 350 and 1000, additional VIA spectra of  $D_5$  SOA, volume-weighted diameter of  $D_5$  SOA size distributions, C/Si and O/Si ratios of  $D_5$  SOA extracted from AMS spectra, list of molecular formulas of major  $D_5$  + OH/Cl oxidation products detected with VIA, and kinetic data used in our KinSim model to estimate the RO<sub>2</sub> fate (PDF)

## AUTHOR INFORMATION

## **Corresponding Authors**

Anita M. Avery — Aerodyne Research, Incorporated, Billerica, Massachusetts 01821, United States; o orcid.org/0000-0002-6130-9664; Email: aavery@aerodyne.com

Andrew T. Lambe — Aerodyne Research, Incorporated,
Billerica, Massachusetts 01821, United States; o orcid.org/
0000-0003-3031-701X; Email: lambe@aerodyne.com

## **Authors**

Mitchell W. Alton — University of Eastern Finland, 70210 Kuopio, Finland; orcid.org/0000-0002-7119-3706 Manjula R. Canagaratna — Aerodyne Research, Incorporated, Billerica, Massachusetts 01821, United States

- Jordan E. Krechmer Aerodyne Research, Incorporated,
   Billerica, Massachusetts 01821, United States; Present
   Address: Jordan E. Krechmer: Bruker Scientific, Billerica,
   Massachusetts 01821, United States
- **Donna T. Sueper** Aerodyne Research, Incorporated, Billerica, Massachusetts 01821, United States
- Nirvan Bhattacharyya Department of Chemical Engineering, University of Texas at Austin, Austin, Texas 78758, United States; orcid.org/0000-0003-3911-6492
- Lea Hildebrandt Ruiz Department of Chemical Engineering, University of Texas at Austin, Austin, Texas 78758, United States; orcid.org/0000-0001-8378-1882
- William H. Brune Department of Meteorology, Pennsylvania State University, University Park, Pennsylvania 16802, United States; orcid.org/0000-0002-1609-4051

Complete contact information is available at: https://pubs.acs.org/10.1021/acsearthspacechem.2c00304

## Notes

The authors declare no competing financial interest.

## ACKNOWLEDGMENTS

This work was supported by the Atmospheric Chemistry Program of the National Science Foundation: Grant AGS-1934352 to Aerodyne Research, Inc., Grant AGS-1934369 to the University of Texas at Austin, and Grant AGS-1934345 to Pennsylvania State University. The authors thank Harald Stark and Megan Claflin (Aerodyne) for helpful discussions.

# REFERENCES

ı

- (1) Tang, X.; Misztal, P. K.; Nazaroff, W. W.; Goldstein, A. H. Siloxanes Are the Most Abundant Volatile Organic Compound Emitted from Engineering Students in a Classroom. *Environ. Sci. Technol. Lett.* **2015**, *2*, 303–307.
- (2) McDonald, B. C.; de Gouw, J. A.; Gilman, J. B.; Jathar, S. H.; Akherati, A.; Cappa, C. D.; Jimenez, J. L.; Lee-Taylor, J.; Hayes, P. L.; McKeen, S. A.; Cui, Y. Y.; Kim, S.-W.; Gentner, D. R.; Isaacman-VanWertz, G.; Goldstein, A. H.; Harley, R. A.; Frost, G. J.; Roberts, J. M.; Ryerson, T. B.; Trainer, M. Volatile chemical products emerging as largest petrochemical source of urban organic emissions. *Science* 2018, 359, 760–764.
- (3) Janechek, N. J.; Hansen, K. M.; Stanier, C. O. Comprehensive atmospheric modeling of reactive cyclic siloxanes and their oxidation products. *Atmos. Chem. Phys.* **2017**, *17*, 8357–8370.
- (4) Coggon, M. M.; McDonald, B. C.; Vlasenko, A.; Veres, P. R.; Bernard, F.; Koss, A. R.; Yuan, B.; Gilman, J. B.; Peischl, J.; Aikin, K. C.; DuRant, J.; Warneke, C.; Li, S.-M.; de Gouw, J. A. Diurnal Variability and Emission Pattern of Decamethylcyclopentasiloxane (D5) from the Application of Personal Care Products in Two North American Cities. *Environ. Sci. Technol.* 2018, 52, 5610–5618.
- (5) Whelan, M. J.; Kim, J. Application of multimedia models for understanding the environmental behavior of volatile methylsiloxanes: Fate, transport, and bioaccumulation. *Integr. Environ. Assess. Manage.* **2022**, *18*, 599–621.
- (6) Atkinson, R. Kinetics of the gas-phase reactions of a series of organosilicon compounds with hydroxyl and nitrate(NO3) radicals and ozone at 297.+-. 2 K. Environ. Sci. Technol. 1991, 25, 863–866.
- (7) Alton, M. W.; Browne, E. C. Atmospheric Chemistry of Volatile Methyl Siloxanes: Kinetics and Products of Oxidation by OH Radicals and Cl Atoms. *Environ. Sci. Technol.* **2020**, *54*, 5992–5999.
- (8) Mao, J.; Ren, X.; Brune, W. H.; Olson, J. R.; Crawford, J. H.; Fried, A.; Huey, L. G.; Cohen, R. C.; Heikes, B.; Singh, H. B.; Blake, D. R.; Sachse, G. W.; Diskin, G. S.; Hall, S. R.; Shetter, R. E. Airborne measurement of OH reactivity during INTEX-B. *Atmos. Chem. Phys.* **2009**, *9*, 163–173.

- (9) Chandramouli, B.; Kamens, R. M. The photochemical formation and gas-particle partitioning of oxidation products of decamethyl cyclopentasiloxane and decamethyl tetrasiloxane in the atmosphere. *Atmos. Environ.* **2001**, *35*, 87–95.
- (10) Wu, Y.; Johnston, M. V. Molecular Characterization of Secondary Aerosol from Oxidation of Cyclic Methylsiloxanes. *J. Am. Soc. Mass Spectrom.* **2016**, 27, 402–9.
- (11) Bzdek, B. R.; Horan, A. J.; Pennington, M. R.; Janechek, N. J.; Baek, J.; Stanier, C. O.; Johnston, M. V. Silicon is a Frequent Component of Atmospheric Nanoparticles. *Environ. Sci. Technol.* **2014**, *48*, 11137–11145.
- (12) Milani, A.; Al-Naiema, I. M.; Stone, E. A. Detection of a secondary organic aerosol tracer derived from personal care products. *Atmos. Environ.* **2021**, *246*, 118078.
- (13) Xu, J.; Harrison, R. M.; Song, C.; Hou, S.; Wei, L.; Fu, P.; Li, H.; Li, W.; Shi, Z. PM2.5-bound silicon-containing secondary organic aerosols (Si-SOA) in Beijing ambient air. *Chemosphere* **2022**, 288, 132377
- (14) Janechek, N. J.; Marek, R. F.; Bryngelson, N.; Singh, A.; Bullard, R. L.; Brune, W. H.; Stanier, C. O. Physical properties of secondary photochemical aerosol from OH oxidation of a cyclic siloxane. *Atmos. Chem. Phys.* **2019**, *19*, 1649–1664.
- (15) Han, C.; Yang, H.; Li, K.; Lee, P.; Liggio, J.; Leithead, A.; Li, S.-M. Secondary Organic Aerosols from OH Oxidation of Cyclic Volatile Methyl Siloxanes as an Important Si Source in the Atmosphere. *Atmos. Chem. Phys.* **2022**, 22, 10827–10839.
- (16) Charan, S. M.; Huang, Y.; Buenconsejo, R. S.; Li, Q.; Cocker, D. R., III; Seinfeld, J. H. Secondary organic aerosol formation from the oxidation of decamethylcyclopentasiloxane at atmospherically relevant OH concentrations. *Atmos. Chem. Phys.* **2022**, 22, 917–928.
- (17) Wingenter, O. W.; Kubo, M. K.; Blake, N. J.; Smith, T. W., Jr.; Blake, D. R.; Rowland, F. S. Hydrocarbon and halocarbon measurements as photochemical and dynamical indicators of atmospheric hydroxyl, atomic chlorine, and vertical mixing obtained during Lagrangian flights. *J. Geophys. Res.* 1996, 101, 4331–4340.
- (18) Baker, A. K.; Sauvage, C.; Thorenz, U. R.; van Velthoven, P.; Oram, D. E.; Zahn, A.; Brenninkmeijer, C. A. M.; Williams, J. Evidence for strong, widespread chlorine radical chemistry associated with pollution outflow from continental Asia. *Sci. Rep.* **2016**, *6*, 36821.
- (19) Wong, J. P. S.; Carslaw, N.; Zhao, R.; Zhou, S.; Abbatt, J. P. D. Observations and impacts of bleach washing on indoor chlorine chemistry. *Indoor Air* **2017**, *27*, 1082–1090.
- (20) Schwartz-Narbonne, H.; Wang, C.; Zhou, S.; Abbatt, J. P.; Faust, J. Heterogeneous Chlorination of Squalene and Oleic Acid. *Environ. Sci. Technol.* **2019**, *53*, 1217–1224.
- (21) Mattila, J. M.; Lakey, P. S. J.; Shiraiwa, M.; Wang, C.; Abbatt, J. P.D.; Arata, C.; Goldstein, A. H.; Ampollini, L.; Katz, E. F.; DeCarlo, P. F.; Zhou, S.; Kahan, T. F.; Cardoso-Saldana, F. J.; Ruiz, L. H.; Abeleira, A.; Boedicker, E. K.; Vance, M. E.; Farmer, D. K. Multiphase Chemistry Controls Inorganic Chlorinated and Nitrogenated Compounds in Indoor Air during Bleach Cleaning. *Environ. Sci. Technol.* 2020, 54, 1730–1739.
- (22) Wu, Y.; Johnston, M. V. Aerosol Formation from OH Oxidation of the Volatile Cyclic Methyl Siloxane (cVMS) Decamethylcyclopentasiloxane. *Environ. Sci. Technol.* **2017**, *51*, 4445–4451.
- (23) Crounse, J. D.; Nielsen, L. B.; Jørgensen, S.; Kjaergaard, H. G.; Wennberg, P. O. Autoxidation of Organic Compounds in the Atmosphere. J. Phys. Chem. Lett. 2013, 4, 3513–3520.
- (24) Zhang, H.; Worton, D. R.; Shen, S.; Nah, T.; Isaacman-VanWertz, G.; Wilson, K. R.; Goldstein, A. H. Fundamental Time Scales Governing Organic Aerosol Multiphase Partitioning and Oxidative Aging. *Environ. Sci. Technol.* **2015**, *49*, 9768–9777.
- (25) Lambe, A. T.; Avery, A. M.; Bhattacharyya, N.; Wang, D. S.; Modi, M.; Masoud, C. G.; Ruiz, L. H.; Brune, W. H. Comparison of secondary organic aerosol generated from the oxidation of laboratory precursors by hydroxyl radicals, chlorine atoms, and bromine atoms in an oxidation flow reactor. *Environ. Sci.: Atmos.* **2022**, *2*, 687–701.

- (26) Rowe, J. P.; Lambe, A. T.; Brune, W. H. Technical Note: Effect of varying the  $\lambda = 185$  and 254 nm photon flux ratio on radical generation in oxidation flow reactors. *Atmos. Chem. Phys.* **2020**, 20, 13417–13424.
- (27) Deming, B. L.; Pagonis, D.; Liu, X.; Day, D. A.; Talukdar, R.; Krechmer, J. E.; de Gouw, J. A.; Jimenez, J. L.; Ziemann, P. J. Measurements of delays of gas-phase compounds in a wide variety of tubing materials due to gas-wall interactions. *Atmos. Meas. Tech.* **2019**, *12*, 3453–3461.
- (28) Lambe, A. T.; Krechmer, J. E.; Peng, Z.; Casar, J. R.; Carrasquillo, A. J.; Raff, J. D.; Jimenez, J. L.; Worsnop, D. R.  $HO_x$  and  $NO_x$  production in oxidation flow reactors via photolysis of isopropyl nitrite, isopropyl nitrite- $d_7$ , and 1,3-propyl dinitrite at  $\lambda = 254$ , 350, and 369 nm. *Atmos. Meas. Tech.* **2019**, 12, 299–311.
- (29) Liu, C.-L.; Smith, J. D.; Che, D. L.; Ahmed, M.; Leone, S. R.; Wilson, K. R. The direct observation of secondary radical chain chemistry in the heterogeneous reaction of chlorine atoms with submicron squalane droplets. *Phys. Chem. Chem. Phys.* **2011**, *13*, 8993.
- (30) Atkinson, R.; Baulch, D. L.; Cox, R. A.; Crowley, J. N.; Hampson, R. F.; Hynes, R. G.; Jenkin, M. E.; Rossi, M. J.; Troe, J. Evaluated kinetic and photochemical data for atmospheric chemistry: Volume III—Gas phase reactions of inorganic halogens. *Atmos. Chem. Phys.* **2007**, *7*, 981–1191.
- (31) Stephens, C. R.; Shepson, P. B.; Steffen, A.; Bottenheim, J. W.; Liao, J.; Huey, L. G.; Apel, E.; Weinheimer, A.; Hall, S. R.; Cantrell, C.; Sive, B. C.; Knapp, D. J.; Montzka, D. D.; Hornbrook, R. S. The relative importance of chlorine and bromine radicals in the oxidation of atmospheric mercury at Barrow, Alaska. *J. Geophys. Res.: Atmos.* 2012, 117, D00R11.
- (32) Faxon, C. B.; Allen, D. T. Chlorine chemistry in urban atmospheres: A review. *Environ. Chem.* **2013**, *10*, 221–233.
- (33) Krechmer, J.; Lopez-Hilfiker, F.; Koss, A.; Hutterli, M.; Stoermer, C.; Deming, B.; Kimmel, J.; Warneke, C.; Holzinger, R.; Jayne, J.; Worsnop, D.; Fuhrer, K.; Gonin, M.; de Gouw, J. Evaluation of a New Reagent-Ion Source and Focusing Ion—Molecule Reactor for Use in Proton-Transfer-Reaction Mass Spectrometry. *Anal. Chem.* **2018**, *90*, 12011–12018.
- (34) de Maré, G. R.; Huybrechts, G. Rate constants for the recombination of CCl3 radicals and for their reactions with Cl, Cl<sub>2</sub> and HCl in the gas phase. *Trans. Faraday Soc.* **1968**, *64*, 1311–1318.
- (35) Burkholder, J. B.; Sander, S. P.; Abbatt, J. P. D.; Barker, J. R.; Cappa, C.; Crounse, J. D.; Dibble, T. S.; Huie, R. E.; Kolb, C. E.; Kurylo, M. J.; Orkin, V. L.; Percival, C. J.; Wilmouth, D. M.; Wine, P. H. Chemical Kinetics and Photochemical Data for Use in Atmospheric Studies; Jet Propulsion Laboratory: Pasadena, CA, 2020; Evaluation Number 19, JPL Publication 19-5.
- (36) Häkkinen, E.; Zhao, J.; Graeffe, F.; Fauré, N.; Krechmer, J.; Worsnop, D.; Timonen, H.; Ehn, M.; Kangasluoma, J. Online measurement of highly oxygenated compounds from organic aerosol. *EGUsphere* **2022**, 2022, 1–29.
- (37) Sueper, D. ToF-AMS Software Downloads; University of Colorado Boulder: Boulder, CO, 2022; http://cires.colorado.edu/jimenez-group/ToFAMSResources/ToFSoftware.
- (38) Canagaratna, M. R.; Jimenez, J. L.; Kroll, J. H.; Chen, Q.; Kessler, S. H.; Massoli, P.; Hildebrandt Ruiz, L.; Fortner, E.; Williams, L. R.; Wilson, K. R.; Surratt, J. D.; Donahue, N. M.; Jayne, J. T.; Worsnop, D. R. Elemental ratio measurements of organic compounds using aerosol mass spectrometry: Characterization, improved calibration, and implications. *Atmos. Chem. Phys.* **2015**, *15*, 253–272.
- (39) Kuwata, M.; Shao, W.; Lebouteiller, R.; Martin, S. T. Classifying organic materials by oxygen-to-carbon elemental ratio to predict the activation regime of Cloud Condensation Nuclei (CCN). *Atmos. Chem. Phys.* **2013**, *13*, 5309–5324.
- (40) Bhattarai, C.; Samburova, V.; Sengupta, D.; Iaukea-Lum, M.; Watts, A. C.; Moosmüller, H.; Khlystov, A. Y. Physical and chemical characterization of aerosol in fresh and aged emissions from open combustion of biomass fuels. *Aerosol Sci. Technol.* **2018**, *52*, 1266–1282.

Meas. Tech. 2022, 15, 1811-1827.

- (41) Brune, W. H. The Chamber Wall Index for Gas-Wall Interactions in Atmospheric Environmental Enclosures. *Environ. Sci. Technol.* **2019**, *53*, 3645–3652.
- (42) He, Y.; Lambe, A. T.; Seinfeld, J. H.; Cappa, C. D.; Pierce, J. R.; Jathar, S. H. Process-Level Modeling Can Simultaneously Explain Secondary Organic Aerosol Evolution in Chambers and Flow Reactors. *Environ. Sci. Technol.* **2022**, *56*, 6262–6273.
- (43) Lambe, A. T.; Onasch, T. B.; Croasdale, D. R.; Wright, J. P.; Martin, A. T.; Franklin, J. P.; Massoli, P.; Kroll, J. H.; Canagaratna, M. R.; Brune, W. H.; Worsnop, D. R.; Davidovits, P. Transitions from Functionalization to Fragmentation Reactions of Laboratory Secondary Organic Aerosol (SOA) Generated from the OH Oxidation of Alkane Precursors. *Environ. Sci. Technol.* **2012**, *46*, 5430–5437.
- (44) Han, C.; Yang, H.; Li, K.; Lee, P.; Liggio, J.; Leithead, A.; Li, S.-M. Secondary organic aerosols from OH oxidation of cyclic volatile methyl siloxanes as an important Si source in the atmosphere. *Atmos. Chem. Phys.* **2022**, *22*, 10827–10839.
- (45) Järvinen, E.; Ignatius, K.; Nichman, L.; Kristensen, T. B.; Fuchs, C.; Hoyle, C. R.; Höppel, N.; Corbin, J. C.; Craven, J.; Duplissy, J.; Ehrhart, S.; El Haddad, I.; Frege, C.; Gordon, H.; Jokinen, T.; Kallinger, P.; Kirkby, J.; Kiselev, A.; Naumann, K.-H.; Petäjä, T.; Pinterich, T.; Prevot, A. S. H.; Saathoff, H.; Schiebel, T.; Sengupta, K.; Simon, M.; Slowik, J. G.; Tröstl, J.; Virtanen, A.; Vochezer, P.; Vogt, S.; Wagner, A. C.; Wagner, R.; Williamson, C.; Winkler, P. M.; Yan, C.; Baltensperger, U.; Donahue, N. M.; Flagan, R. C.; Gallagher, M.; Hansel, A.; Kulmala, M.; Stratmann, F.; Worsnop, D. R.; Möhler, O.; Leisner, T.; Schnaiter, M. Observation of viscosity transition in  $\alpha$ -pinene secondary organic aerosol. *Atmos. Chem. Phys.* **2016**, *16*, 4423–4438.
- (46) DeCarlo, P. F.; Slowik, J. G.; Worsnop, D. R.; Davidovits, P.; Jimenez, J. L. Particle morphology and density characterization by combined mobility and aerodynamic diameter measurements. Part 1: Theory. *Aerosol Sci. Technol.* **2004**, *38*, 1185–1205.
- (47) Chen, Y.; Park, Y.; Kang, H. G.; Jeong, J.; Kim, H.Identification of Secondary Organosiloxane Aerosol (SOSA) Using Aerosol Mass Spectrometry. *Proceedings of the 11th International Aerosol Conference*; Athens, Greece, Sept 4–9, 2022.
- (48) Takegawa, N.; Miyakawa, T.; Kawamura, K.; Kondo, Y. Contribution of Selected Dicarboxylic and  $\omega$ -Oxocarboxylic Acids in Ambient Aerosol to the m/z 44 Signal of an Aerodyne Aerosol Mass Spectrometer. *Aerosol Sci. Technol.* **2007**, *41*, 418–437.
- (49) Makens, R. F.; Eversole, W. G. Kinetics of the Thermal Decomposition of Ethyl Formate. *J. Am. Chem. Soc.* **1939**, *61*, 3203–3206.
- (50) Alton, M. W.; Browne, E. C. Atmospheric Degradation of Cyclic Volatile Methyl Siloxanes: Radical Chemistry and Oxidation Products. *ACS Environ. Au* **2022**, *2*, 263–274.
- (51) Wang, D. S.; Hildebrandt Ruiz, L. Secondary organic aerosol from chlorine-initiated oxidation of isoprene. *Atmos. Chem. Phys.* **2017**, *17*, 13491–13508.
- (52) Wang, D. S.; Hildebrandt Ruiz, L. Chlorine-initiated oxidation of *n*-alkanes under high-NO<sub>x</sub> conditions: Insights into secondary organic aerosol composition and volatility using a FIGAERO–CIMS. *Atmos. Chem. Phys.* **2018**, *18*, 15535–15553.
- (53) Maricq, M. M.; Szente, J. J.; Kaiser, E. W.; Shi, J. Reaction of Chlorine Atoms with Methylperoxy and Ethylperoxy Radicals. *J. Phys. Chem.* **1994**, *98*, 2083–2089.
- (54) Atkinson, R.; Baulch, D. L.; Cox, R. A.; Crowley, J. N.; Hampson, R. F., Jr.; Hynes, R. G.; Jenkin, M. E.; Kerr, J. A.; Rossi, M. J.; Troe, J. Summary of Evaluated Kinetic and Photochemical Data for Atmospheric Chemistry; Centre for Atmospheric Science, University of Cambridge: Cambridge, U.K., 2001.
- (55) Riva, M.; Rantala, P.; Krechmer, J. E.; Peräkylä, O.; Zhang, Y.; Heikkinen, L.; Garmash, O.; Yan, C.; Kulmala, M.; Worsnop, D.; Ehn, M. Evaluating the performance of five different chemical ionization techniques for detecting gaseous oxygenated organic species. *Atmos. Meas. Tech.* **2019**, *12*, 2403–2421.
- (56) Heald, C. L.; Kroll, J. H.; Jimenez, J. L.; Docherty, K. S.; Decarlo, P. F.; Aiken, A. C.; Chen, Q.; Martin, S. T.; Farmer, D. K.;

- Artaxo, P. A simplified description of the evolution of organic aerosol composition in the atmosphere. *Geophys. Res. Lett.* **2010**, *37*, L08803. (57) Li, H.; Almeida, T. G.; Luo, Y.; Zhao, J.; Palm, B. B.; Daub, C. D.; Huang, W.; Mohr, C.; Krechmer, J. E.; Kurtén, T.; Ehn, M. Fragmentation inside proton-transfer-reaction-based mass spectrometers limits the detection of ROOR and ROOH peroxides. *Atmos.*
- (58) Peng, Z.; Jimenez, J. L. KinSim: A Research-Grade, User-Friendly, Visual Kinetics Simulator for Chemical-Kinetics and Environmental-Chemistry Teaching. *J. Chem. Educ.* **2019**, *96*, 806–811
- (59) Baulch, D. L.; Duxbury, J.; Grant, S. J. Evaluated kinetic data for high temperature reactions. Volume 4. Homogeneous gas phase reactions of halogen- and cyanide- containing species. *J. Phys. Chem. Ref. Data* 1981, 10, 723.
- (60) DeMore, W. B.; Sander, S. P.; Golden, D. M.; Hampson, R. F.; Kurylo, M. J.; Howard, C. J.; Ravishankara, A. R.; Kolb, C. E.; Molina, M. J.*Chemical Kinetics and Photochemical Data for Use in Stratospheric Modeling*; Jet Propulsion Laboratory: Pasadena, CA, 1997; Evaluation Number 12, JPL Publication 97-4.
- (61) Ziemann, P. J.; Atkinson, R. Kinetics, products, and mechanisms of secondary organic aerosol formation. *Chem. Soc. Rev.* **2012**, *41*, 6582–6605.
- (62) Orlando, J. J.; Tyndall, G. S. Laboratory studies of organic peroxy radical chemistry: An overview with emphasis on recent issues of atmospheric significance. *Chem. Soc. Rev.* **2012**, *41*, 6294–6317.
- (63) Fittschen, C. The reaction of peroxy radicals with OH radicals. *Chem. Phys. Lett.* **2019**, 725, 102–108.
- (64) Fu, Z.; Xie, H.-B.; Elm, J.; Guo, X.; Fu, Z.; Chen, J. Formation of Low-Volatile Products and Unexpected High Formaldehyde Yield from the Atmospheric Oxidation of Methylsiloxanes. *Environ. Sci. Technol.* **2020**, *54*, 7136–7145.
- (65) Presto, A.; Miracolo, M.; Donahue, N.; Robinson, A. Secondary organic aerosol formation from high-NO x photo-oxidation of low volatility precursors: *n*-Alkanes. *Environ. Sci. Technol.* **2010**, 44, 2029—2034.
- (66) Loza, C. L.; Craven, J. S.; Yee, L. D.; Coggon, M. M.; Schwantes, R. H.; Shiraiwa, M.; Zhang, X.; Schilling, K. A.; Ng, N. L.; Canagaratna, M. R.; Ziemann, P. J.; Flagan, R. C.; Seinfeld, J. H. Secondary organic aerosol yields of 12-carbon alkanes. *Atmos. Chem. Phys.* **2014**, *14*, 1423–1439.
- (67) Lambe, A. T.; Onasch, T. B.; Croasdale, D. R.; Wright, J. P.; Martin, A. T.; Franklin, J. P.; Massoli, P.; Kroll, J. H.; Canagaratna, M. R.; Brune, W. H.; Worsnop, D. R.; Davidovits, P. Transitions from functionalization to fragmentation reactions of secondary organic aerosol (SOA) generated from the laboratory OH oxidation of alkane precursors. *Environ. Sci. Technol.* **2012**, *46*, 5430–5437.
- (68) Lambe, A. T.; Chhabra, P. S.; Onasch, T. B.; Brune, W. H.; Hunter, J. F.; Kroll, J. H.; Cummings, M. J.; Brogan, J. F.; Parmar, Y.; Worsnop, D. R.; Kolb, C. E.; Davidovits, P. Effect of oxidant concentration, exposure time, and seed particles on secondary organic aerosol chemical composition and yield. *Atmos. Chem. Phys.* **2015**, *15*, 3063–3075.
- (69) Tkacik, D. S.; Presto, A. A.; Donahue, N. M.; Robinson, A. L. Secondary organic aerosol formation from intermediate-volatility organic compounds: Cyclic, linear, and branched alkanes. *Environ. Sci. Technol.* **2012**, *46*, 8773–8781.
- (70) Wang, Z.; Kowal, S. F.; Carslaw, N.; Kahan, T. F. Photolysis-driven indoor air chemistry following cleaning of hospital wards. *Indoor Air* **2020**, *30*, 1241–1255.
- (71) Jayne, J. T.; Leard, D. C.; Zhang, X. F.; Davidovits, P.; Smith, K. A.; Kolb, C. E.; Worsnop, D. R. Development of an aerosol mass spectrometer for size and composition analysis of submicron particles. *Aerosol Sci. Technol.* **2000**, 33, 49–70.
- (72) Canagaratna, M. R.; Jayne, J. T.; Jimenez, J. L.; Allan, J. D.; Alfarra, M. R.; Zhang, Q.; Onasch, T. B.; Drewnick, F.; Coe, H.; Middlebrook, A.; Delia, A.; Williams, L. R.; Trimborn, A. M.; Northway, M. J.; DeCarlo, P. F.; Kolb, C. E.; Davidovits, P.; Worsnop, D. R. Chemical and microphysical characterization of ambient

aerosols with the aerodyne aerosol mass spectrometer. *Mass Spectrom. Rev.* **2007**, *26*, 185–222.

- (73) Katz, E. F.; Lunderberg, D. M.; Brown, W. L.; Day, D. A.; Jimenez, J. L.; Nazaroff, W. W.; Goldstein, A. H.; DeCarlo, P. F. Large Emissions of Low-Volatility Siloxanes during Residential Oven Use. *Environ. Sci. Technol. Lett.* **2021**, *8*, 519–524.
- (74) Cross, E.; Slowik, J.; Davidovits, P.; Allan, J.; Worsnop, D.; Jayne, J.; Lewis, D.; Canagaratna, M.; Onasch, T. Laboratory and Ambient Particle Density Determinations Using Light Scattering in Conjunction with Aerosol Mass Spectrometry. *Aerosol Sci. Technol.* **2007**, *41*, 343–359.